Supplement of Clim. Past, 22, 1223–1240, 2026
https://doi.org/10.5194/cp-22-1223-2026-supplement

Climate of the Past Open Access EGU

Supplement of

The Marine Isotopic Stage 7: a relic of the "41 ka world"? Perspectives from a global-scale sea-surface temperature synthesis

Etienne Legrain et al.

Correspondence to: Etienne Legrain (etienne.legrain@vub.be)

Supplementary Information

S1. Spatio-temporal evolution of individual SST records

S1.1 North Pacific basin

The MIS 7 SST evolution in the North Pacific (>10°N) is reconstructed from 17 records across 10 sites distributed along the basin's eastern (ODP-1012, ODP-1020, LPAZ-21P), central (MD01-2416), and western sectors (all other cores) (Fig. S1). In the eastern sector, MIS 7 is characterized by a two-warm-phase structure clearly preserved in the $U^{K'}_{37}$-SST reconstructions. Notably, the MIS 7c appears warmer than MIS 7e. The northern central Pacific, represented by MD01-2416, shows an intense MIS 7e relative to MIS 7c, although all SSTs remain below PI values. Western Pacific sites (e.g. ODP-1144, ODP-1146, U1429) exhibit more complex variability, with a blurred MIS 7 morphology. A high-frequency variability component appears to be superimposed on the classical two-peak structure of MIS 7. These sites register a warming trend toward younger ages, with MIS 7c exceeding MIS 7e in amplitude. Sites with multiple SST reconstructions (e.g. MD05-2901, ODP-1146) often show notable differences in magnitude and structure, particularly between UK_{37}'- and $\delta^{18}O_p$-derived records. At site U1429, for example, inter-proxy trends are consistent, but amplitude discrepancies are substantial: the Mg/Ca-based reconstruction indicates anomalously warm interglacial values exceeding +6°C above PI, whereas both $\delta^{18}O_p$- and $U^{K'}_{37}$-based estimates remain within ±2°C.

S1.2 North Atlantic basin

The MIS 7 SST variability in the North Atlantic (>0°) is reconstructed from 25 records across 15 sites spanning the western (ODP-1059), central (U1313, ODP-607, V30-97), and eastern sectors of the basin (all other cores) (Fig. S1). The SST evolution is marked by a well-defined two-peak structure, typical of MIS 7. In several records (e.g. ODP1059, SU90-39, U1385), a three-peak pattern corresponding to MIS 7e, 7c, and 7a can also be distinguished. In the central Atlantic, the MIS 7c peak is similar to, or warmer than MIS 7e, though both remain below PI values (typically inferior to –1°C). In the western Atlantic, the $\delta^{18}O_p$ record displays a three-peak morphology, with MIS 7e slightly more pronounced than 7c and 7a, and SSTs reaching PI levels. In the eastern part of the basin, MIS 7e and 7c are generally of comparable magnitude. Iberian margin sites reach PI values, while more northerly sites (e.g. ODP 980) show SSTs exceeding PI by up to 4°C. Sites with multiple proxies reveal substantial mismatches in both amplitude and structure, particularly between MAT- and $\delta^{18}O_p$-derived SSTs. At site U1385, for example, the MAT reconstruction shows a strongly amplified MIS 7e, whereas the $\delta^{18}O_p$ record captures similar maxima for both MIS 7e and 7c, making MIS 7c appear relatively warmer than in the MAT record.

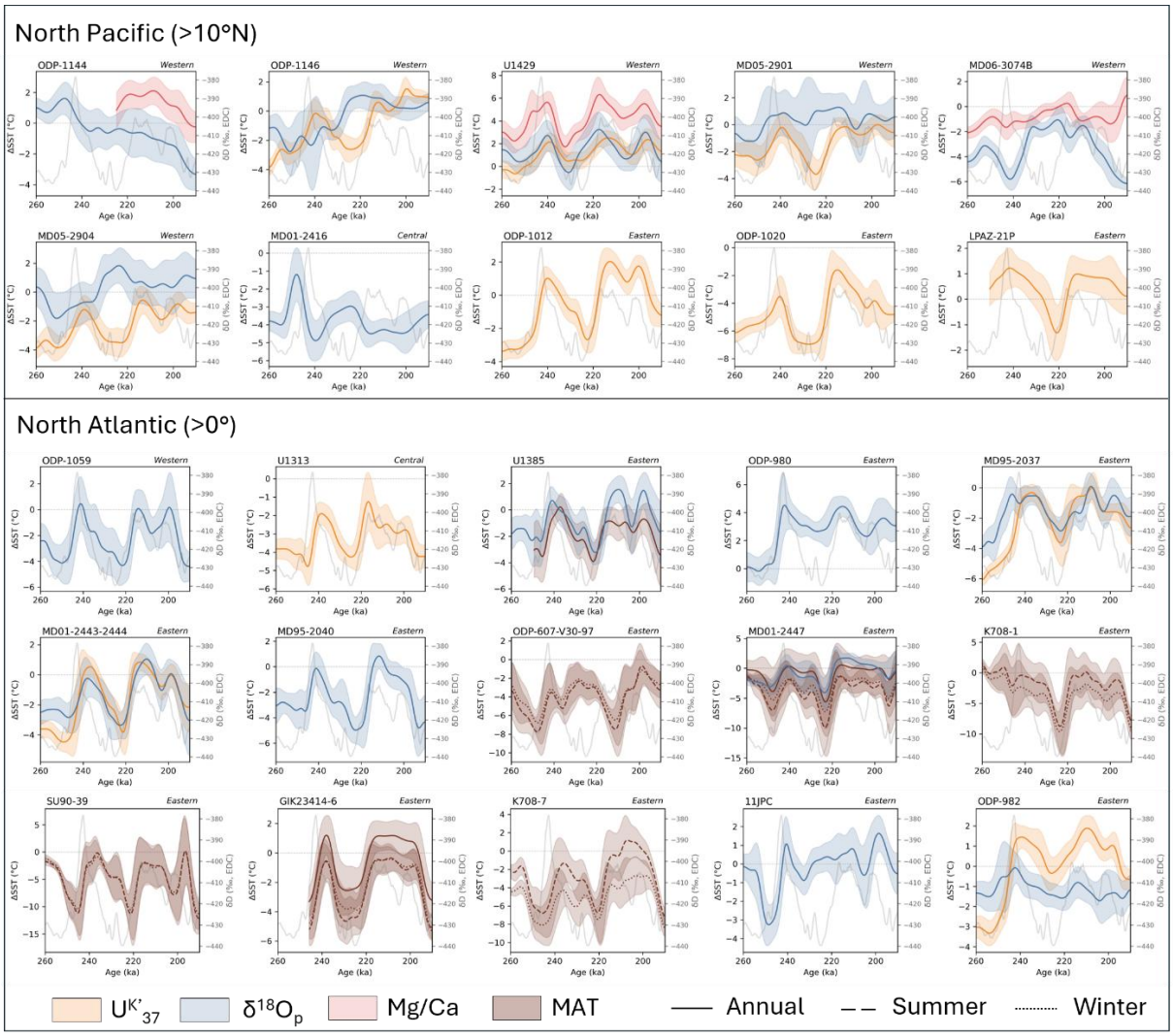

Fig. S1: **SST anomalies relative to PI for sites located in the North Pacific (>10°N) and North Atlantic (>0°)**. Colors refers to the SST proxies used: $U^{k'}_{37}$ (orange), $\delta^{18}O_p$ (blue), Mg/Ca (pink) and Modern Analog Technique (MAT) (brown). The grey curve is the δD record from the EPICA Dome C (EDC) ice core (Jouzel et al., 2007) on the AICC2023 timescale (Bouchet et al., 2023), added for visual comparison. The horizontal dotted grey line corresponds to the PI value at the location of each core. SST anomalies are representative of annual (solid lines), summer (dashed lines) or winter (dotted lines) signal. All records are time-binned every 500 years to consider age uncertainties. The colored envelopes represent the 1σ uncertainty computed from age and SST uncertainties. The top right mention refers to the sub-region of the oceanic basin, as described in the main text.

S1.3 Equatorial pacific basin

The MIS 7 SST evolution in the Equatorial Pacific (10°N–10°S) is reconstructed from 25 records across 18 sites distributed across the eastern (8 cores), central (ML1208-16BB), and western sectors (7 cores) of the basin, along with two additional sites from the China Sea (ODP-1143 and MD97-2141) (Fig. S2). The overall structure of SST variability is highly heterogeneous, with substantial spatial differences in amplitude and morphology of substages. In the eastern Equatorial Pacific, SST signals are particularly variable. For example, two $\delta^{18}O_p$-based SST records located only ~1,500 km apart display opposite trends over the 260–190 ka interval: a gradual cooling in RC13-110 versus a gradual warming in ODP-677. Additionally, some records show a flat MIS 7 signal (e.g. V19-30, with <1°C of variability between 260 and 210 ka), whereas others (e.g. ODP-806) record a TIIIa amplitude exceeding 3°C. Overall, SSTs in this region remain close to or slightly colder than PI throughout the interval. In

the central Pacific, the $\delta^{18}O_p$-SST reconstruction from ML1208-16BB displays low variability (<2°C) throughout MIS 7. MIS 7c appears in most of records warmer than MIS 7e, but both peaks are ~3°C below PI values. In the western Equatorial Pacific, the classical bi-phase structure of MIS 7 is more clearly expressed. In some records (e.g. MD05-2925), both peaks are of similar magnitude, while in others (e.g. ODP-871), MIS 7c appears slightly warmer. Sites with multi-proxy reconstructions further reveal structural and amplitude discrepancies. For instance, at site KX97322-4, the $\delta^{18}O_p$-SST record shows no significant variability, whereas the Mg/Ca-based reconstruction exhibits a distinct two-peak pattern with SSTs approaching PI values during MIS 7e and 7c. In the China Sea, both records indicate a more pronounced MIS 7c compared to MIS 7e, although their absolute SST anomalies relative to PI differ across proxies.

S1.4 Indian Ocean basin

The MIS 7 SST evolution in the Indian Ocean is reconstructed from 14 records across 10 sites distributed across the southern (3 cores), eastern (2 cores), western (1 core), and northern (4 cores) sectors of the basin (Fig. S2). The SST signal is characterized by large heterogeneity, which does not appear to follow a clear spatial pattern across sub-basins. While all records show a distinct MIS 7e peak, with temperatures ranging approximately ~2°C relative to PI, the expression of TIIIa and MIS 7c is more variable. Some cores display a two-peak morphology (e.g. MD04-2881, MD98-2152), whereas others do not record any warming during MIS 7c (e.g. RC27-61). In addition, some records show a more intense MIS 7a compared to 7c (e.g. ODP-722), or exhibit a delayed MIS 7c peak centered around 210 ka (e.g. MD04-2881). Interestingly, the only core located within the Agulhas Current region (MD96-2077) does not record any distinct TIIIa event. Instead, MIS 7 is expressed as a continuous warm plateau. At the three-proxy site RC11-120, major discrepancies are observed between the $\delta^{18}O_p$-derived SST and both the MAT- and Mg/Ca-based reconstructions, highlighting substantial proxy-related differences in this region.

S1.5 Other seas

The “Other seas” category includes four sites from the Caribbean Sea (ODP-1002, ODP-999, MD02-2575, and MD94-480) and one from the Mediterranean (PRGL1) (Fig. S2). In the Caribbean Sea, all four records consistently show a well-defined MIS 7e, with SST amplitudes reaching up to 5°C, except for ODP-1002, which displays an exceptional amplitude during TIII (~11°C), the highest value observed across the entire dataset. In contrast, TIIIa is not recorded at these sites; MIS 7 is instead expressed as a gradual cooling trend from MIS 7a toward MIS 6. In the Mediterranean Sea, the $\delta^{18}O_p$-SST record from PRGL1 shows a two-peak morphology, slightly shifted toward younger ages compared to the broader dataset (~230 ka and 210 ka). The $U^{K'}_{37}$-SST reconstruction at the same site exhibits a flatter pattern, highlighting discrepancies between different SST proxies in this marginal sea.

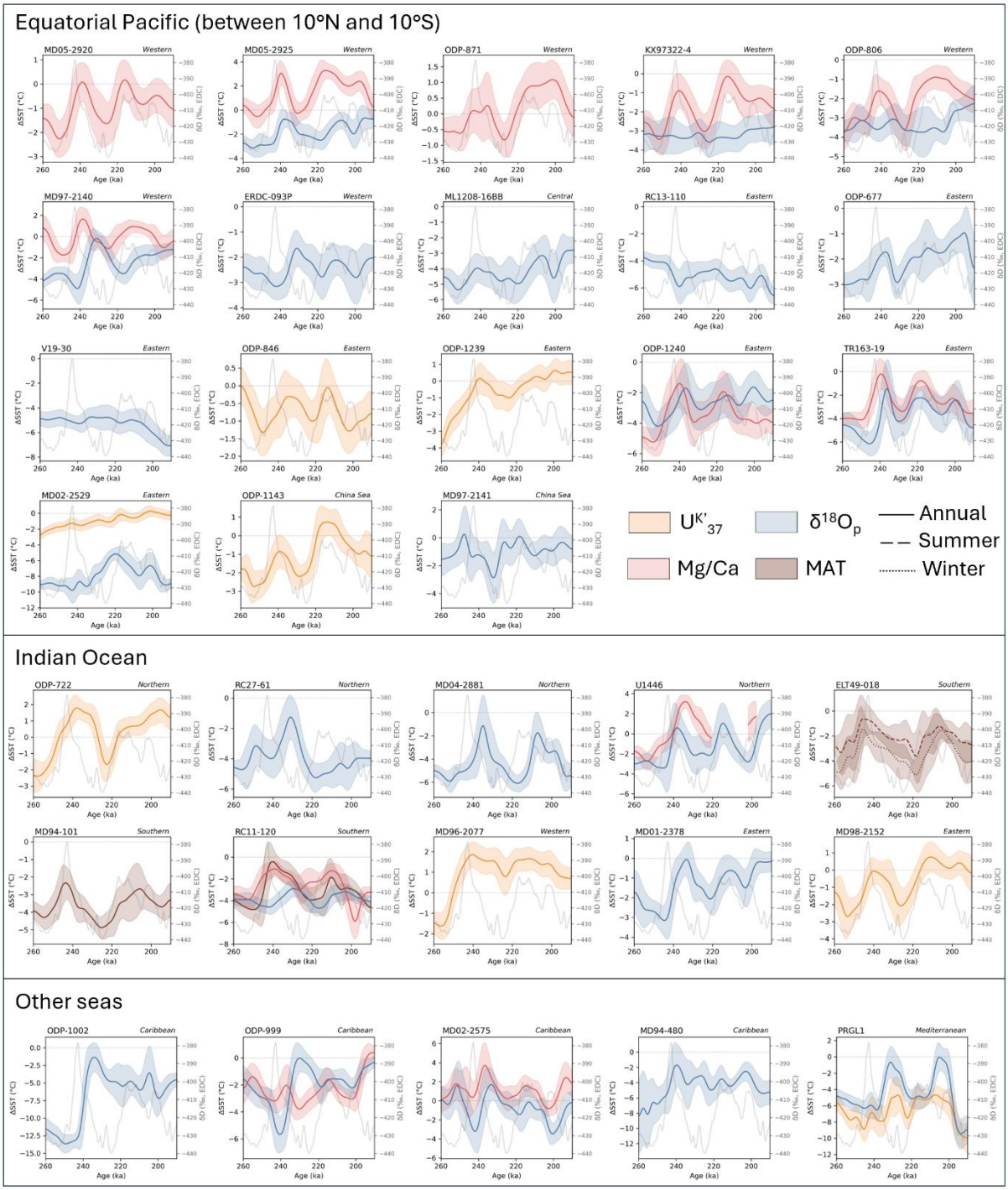

80 Fig. S2: Same as Fig. S1 but for Equatorial Pacific (between 10°N and 10°S), Indian Ocean and other seas.

S1.6 South Atlantic basin

The MIS 7 SST evolution in the South Atlantic is reconstructed from 28 records across 20 sites, the majority of which (15/20) are located along the central and eastern margin of the basin between 20°S and 53°S (Fig. S3). The remaining five sites are situated in the equatorial zone, between –1°S and –9°S. The equatorial sites display a
85 coherent pattern, with well-defined MIS 7e and 7c peaks, the latter being more amplified. SSTs during MIS 7e and 7c are generally 1–2°C warmer than PI in this area. The amplitude of TIIIa varies notably, ranging from values

similar to TIII (e.g. 2°C in GeoB1113-4) to significantly weaker expressions (e.g. 2°C vs. 6°C in ODP-662). Across the broader South Atlantic, no clear latitudinal gradient in SST variability is evident. Instead, two dominant MIS 7 morphologies are observed. The first includes records with a well-defined MIS 7e, more pronounced than MIS 7c. The second group includes records with flatter and noisier SST trends, where MIS 7e and 7c are not clearly distinguishable as the warmest phases of the interval (e.g. TN057-06, RC13-228). This apparent proxy-dependence, illustrated by contrasting results at GeoB1028-5 depending on the SST proxy used, suggests that reconstruction method plays a significant role in shaping interpretations of MIS 7 SST variability in this region.

S1.7 South Pacific basin

The South Pacific (>10°S) is represented by nine records from seven distinct sites, distributed across the eastern (GeoB3327-5) and western (all other cores) sectors of the basin (Fig. S3). The only site from the southeastern Pacific (GeoB3327-5) exhibits a clear two-peak structure, with MIS 7c more pronounced (+1°C relative to PI) than MIS 7e (similar to PI), which remains close to PI levels. In the western South Pacific, SST records generally show well-defined TIII and MIS 7e peaks, with the exception of ODP-1125. These peaks are of similar or even greater amplitude than MIS 7c. Compared to other basins, the South Pacific records are relatively consistent in structure, although inter-proxy biases remain apparent. For example, at site SO136-GC3, the morphology of $\delta^{18}O_p$- and $U^{K'}_{37}$-based SST estimates differ substantially.

S1.8 Selection of records

We excluded a few records from the stacking process (see Section 3.1 in the main text). Specifically, we removed records that (1) display a pattern of variability markedly different from the regional trend, or (2) show SST estimates that strongly disagree with those derived from another proxy at the same site. This includes 14 $\delta^{18}O_p$-based SST records (ODP-1144, MD01-2416, MD05-2904, KX97322-4, ODP-806, MD97-2140, RC13-110, V19-30, MD02-2529, MD97-2141, ODP-999, TN057-06, GeoB1028-5 and SO136-GC3) and one Mg/Ca-based SST record (ODP-1144).

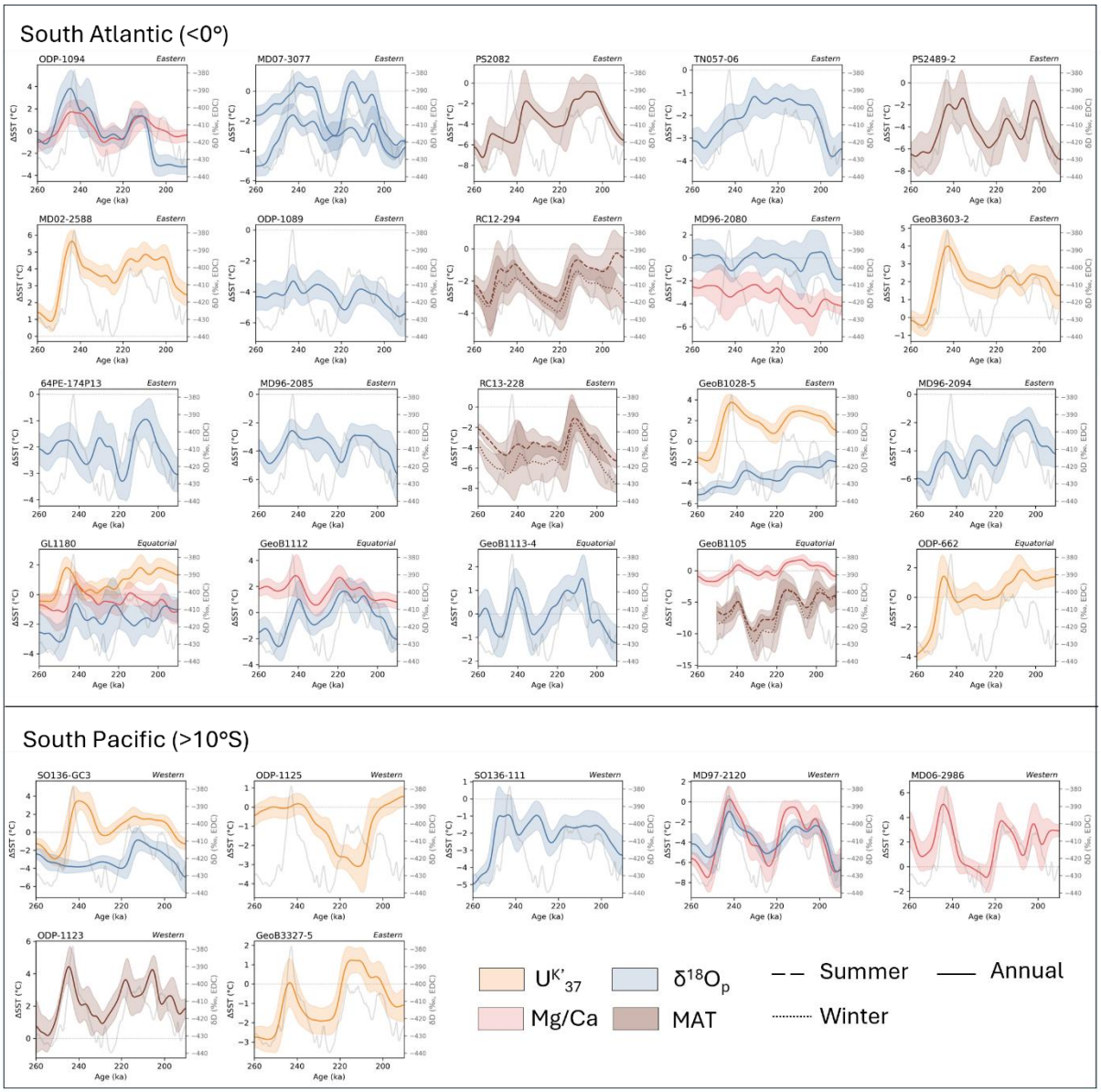

Fig. S3: Same as Fig. S1 but for South Atlantic (<0°) and South Pacific (>10°S). The two $\delta^{18}O_p$ – SST records of the MD07-3077 core correspond to SST records from two different species of planktonic foraminifera: *Neogloboquadrina pachyderma* (top curve) and *Globigerina bulloides* (bottom curve) *(this study)*.

S2. Chronologies

Chronologies were established by aligning oceanic basins onto ice core and speleothem archives, that differs among the considered basins. In the North Atlantic and Mediterranean basin, the records are aligned to the Greenland Synthetic Curve (Barker et al., 2011). In the North and Equatorial Pacific basin, the alignment procedure differs slightly between sub-basins. The North- and Equatorial-East Pacific records are aligned to the synthetic Greenland temperature record (GLT_syn). In contrast, the North- and Equatorial-West Pacific records are aligned to a reference record, itself aligned to the Sanbao speleothem record (Cheng et al., 2016). In the South Atlantic, South Pacific and Indian Ocean basins, the records are aligned onto reference records, themself aligned to the EPICA Dome C ice isotopes records (Jouzel et al., 2007). Finally, the Caribbean records are aligned through a

stepwise procedure. Core MD02-2575 was first aligned to U1385 using benthic $\delta^{18}O$, as direct alignment of SST signals with North Atlantic SST records was not feasible due to large discrepancies between the records. Subsequently, ODP-999 and ODP-1002 were aligned to MD02-2575 using both Mg/Ca and $\delta^{18}O$ SST records.

Fig. S4 presents the alignment of each site (blue curve) to its reference (black curve).

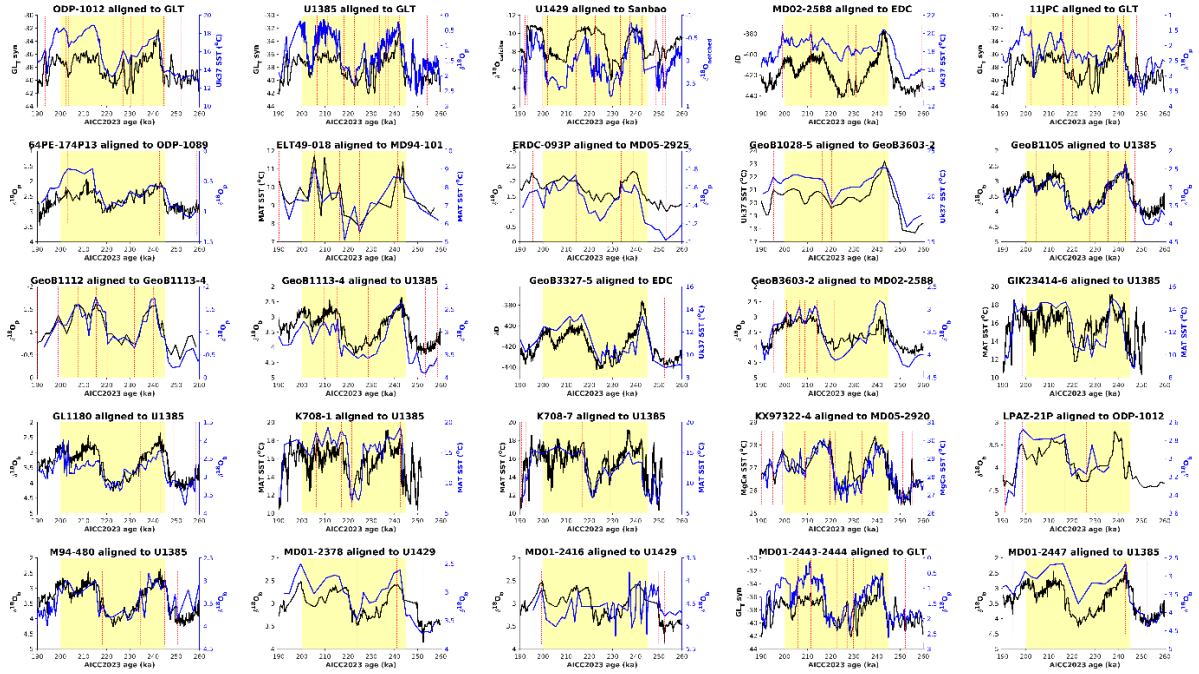

Fig. S4: Alignments of the SST sites used in this study. For each plot, the blue line represents the record used to align to the reference (black line). The dotted vertical red lines are the tie-points as defined in the AnalySeries software (Paillard et al., 1996). The light yellow area in each plot approximately identifies the MIS 7.

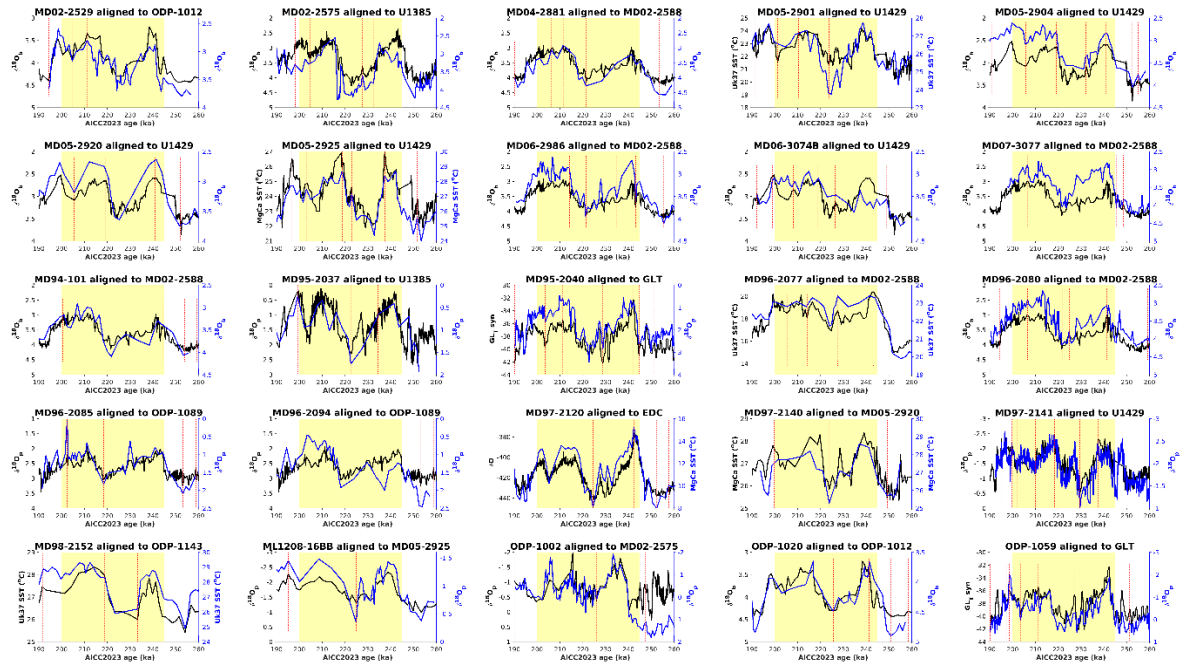

Fig. S4 (continued)

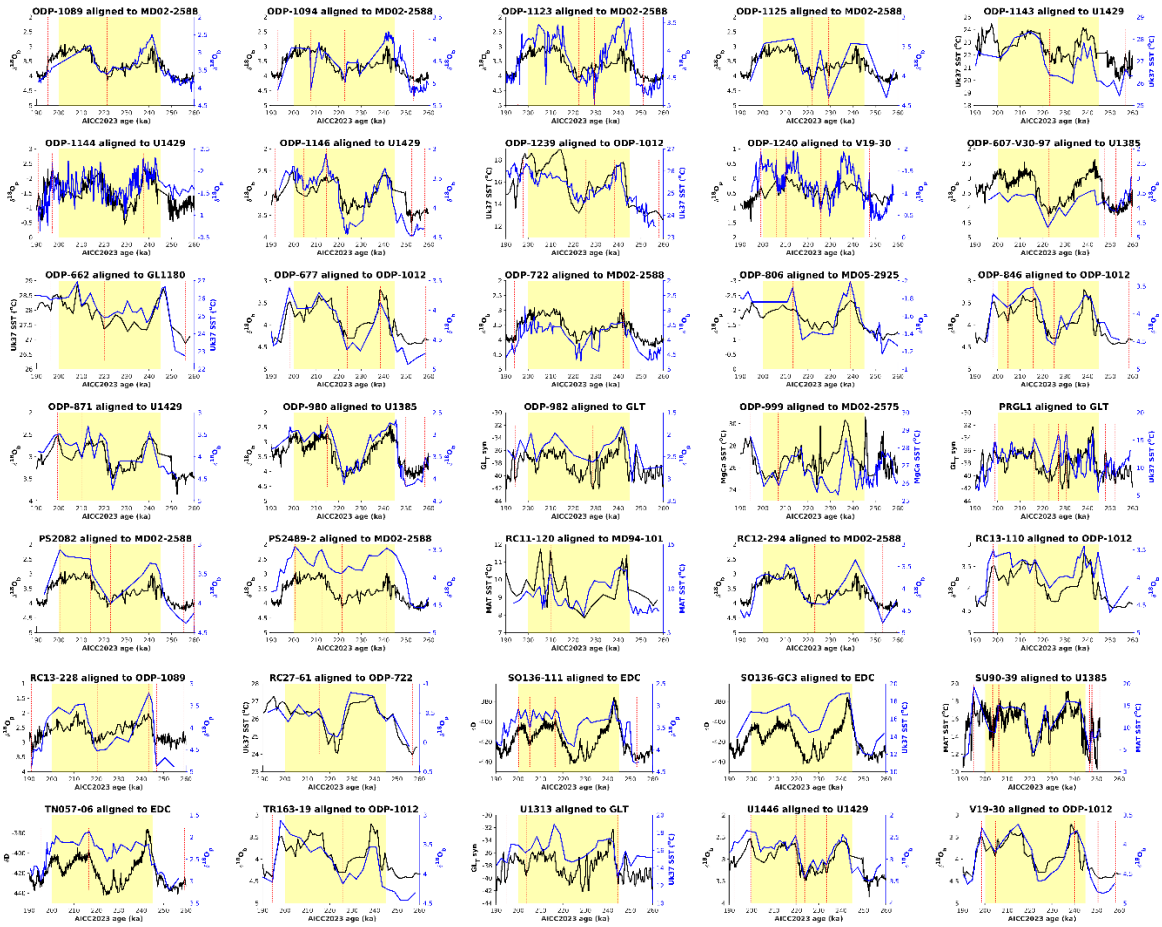

135

Fig. S4 (continued)

Table S1: Locations, available proxies used in this study, SST type and original references of the sites used in this study. All UK'_{37} records are considered to reflect annual conditions, except for ODP-982. Due to its specific location above 48°N in the North Atlantic, and following the authors' recommendation, this record is interpreted as reflecting seasonal variations (Tierney and Tingley, 2018).

Core	Lat (°)	Long (°)	Elevation (m)	Basin	Method (SST)	Species	SST type	Mean resolution (kyr)	Reference
11JPC	56.23	-27.65	-2707	North Atlantic	$\delta^{18}O$	*G. bulloides*	Annual	0.95	[1]
64PE-174P13	-29.76	2.40	-2912	South Atlantic	$\delta^{18}O$	*G. ruber*	Seasonal	2.75	[2]
ELT49-018	-46.05	90.16	-3282	Indian	MAT	*Na*	Seasonal	1.51	[3]
ERDC-093P	-2.24	157.01	-1604	Equatorial Pacific	$\delta^{18}O$	*T. sacculifer*	Annual	1.80	[4]
GeoB1028-5	-20.10	9.19	-2209	South Atlantic	$\delta^{18}O$	*Bulk*	Annual	1.70	[5]
GeoB1028-5	-20.10	9.19	-2209	South Atlantic	$U^{K'}_{37}$	*Na*	Annual	2.09	[6]
GeoB1105	-1.67	-12.43	-3231	Equatorial Atlantic	MAT	*Na*	Seasonal	1.61	[7]
GeoB1105	-1.67	-12.43	-3225	Equatorial Atlantic	Mg/Ca	*T. sacculifer*	Annual	2.19	[8]
GeoB1112	-5.77	-10.75	-3122	Equatorial Atlantic	$\delta^{18}O$	*G. ruber*	Annual	1.94	[5]
GeoB1112	-5.77	-10.75	-3122	Equatorial Atlantic	Mg/Ca	*T. sacculifer*	Annual	1.94	[8]
GeoB1113-4	-5.75	-11.04	-2374	Equatorial Atlantic	$\delta^{18}O$	*G. ruber*	Annual	1.63	[9]
GeoB3327-5	-43.24	-79.99	-3531	South Pacific	$U^{K'}_{37}$	*Na*	Annual	3.23	[10]
GeoB3603-2	-35.13	17.54	-2840	South Atlantic	$U^{K'}_{37}$	*Na*	Annual	1.76	[11]
GIK23414-6	53.54	-20.29	-2201	North Atlantic	MAT	*Na*	Seasonal	1.61	[12]
GL1180	-8.45	-33.55	-1037	Equatorial Atlantic	$\delta^{18}O$	*G. ruber*	Annual	2.00	[13]
GL1180	-8.45	-33.55	-1037	Equatorial Atlantic	Mg/Ca	*G. ruber*	Annual	2.00	[13]
GL1180	-8.45	-33.55	-1037	Equatorial Atlantic	$U^{K'}_{37}$	*Na*	Annual	2.00	[14]

K708-1	50.00	-23.73	-4053	North Atlantic	MAT	*Na*	Seasonal	1.00	[15]
K708-7	53.93	-24.08	-3502	North Atlantic	MAT	*Na*	Seasonal	2.00	[16]
KX97322-4	-0.03	159.25	-2362	Equatorial Pacific	$\delta^{18}O$	*G. ruber*	Annual	0.54	[17]
KX97322-4	-0.03	159.25	-2362	Equatorial Pacific	Mg/Ca	*G. ruber*	Annual	2.84	[17]
LPAZ-21P	22.98	-109.47	-624	North Pacific	$U^{K'}_{37}$	*Na*	Annual	1.63	[18]
M94-480	23.80	-87.01	-730.3	Other	$\delta^{18}O$	*G. ruber*	Annual	1.29	[19]
MD01-2378	-13.08	121.79	-1783	Indian	$\delta^{18}O$	*G. ruber*	Annual	2.32	[20]
MD01-2416	51.27	167.73	-2317	North Pacific	$\delta^{18}O$	*N. pachyderma*	Annual	2.00	[21]
MD01-2443-2444	37.69	-10.15	-2790	North Atlantic	$\delta^{18}O$	*G. bulloides*	Annual	0.38	[22]
MD01-2443-2444	37.69	-10.15	-2790	North Atlantic	$U^{K'}_{37}$	*Na*	Annual	0.41	[22]
MD01-2447	42.15	-9.66	-2080	North Atlantic	$\delta^{18}O$	*G. bulloides*	Annual	1.47	[23]
MD01-2447	42.15	-9.66	-2080	North Atlantic	MAT	*Na*	Seasonal	2.70	[24]
MD02-2529	8.21	-84.12	-1619	Equatorial Pacific	$\delta^{18}O$	*G. ruber*	Annual	1.22	[25]
MD02-2529	8.21	-84.12	-1619	Equatorial Pacific	$U^{K'}_{37}$	*Na*	Annual	1.22	[25]
MD02-2575	29.00	-87.12	-847	Other	$\delta^{18}O$	*G. ruber*	Annual	0.69	[26]
MD02-2575	29.00	-87.12	-847	Other	Mg/Ca	*G. ruber*	Annual	0.76	[26]
MD02-2588	-41.20	25.50	-2907	South Atlantic	$U^{K'}_{37}$	*Na*	Annual	0.80	[27]
MD04-2881	22.20	63.08	-2387	Indian	$\delta^{18}O$	*G. ruber*	Annual	2.57	[28]
MD05-2901	14.38	110.74	-1454	North Pacific	$\delta^{18}O$	*G. ruber*	Annual	0.91	[29]
MD05-2901	14.38	110.74	-1454	North Pacific	$U^{K'}_{37}$	*Na*	Annual	0.96	[29]
MD05-2904	19.46	116.25	-2066	North Pacific	$\delta^{18}O$	*G. ruber*	Annual	0.37	[30]
MD05-2904	19.46	116.25	-2066	North Pacific	$U^{K'}_{37}$	*Na*	Annual	0.73	[30]
MD05-2920	-2.86	144.53	-1849	Equatorial Pacific	Mg/Ca	*G. ruber*	Annual	1.65	[31]
MD05-2925	-9.34	151.46	-1661	Equatorial Pacific	$\delta^{18}O$	*G. ruber*	Annual	1.12	[32]
MD05-2925	-9.34	151.46	-1661	Equatorial Pacific	Mg/Ca	*G. ruber*	Annual	1.12	[32]

MD06-2986	-43.45	167.90	-1477	South Pacific	Mg/Ca	*G. bulloides*	Annual	1.29	[33]
MD06-3074B	17.01	124.81	-2510	North Pacific	$\delta^{18}O$	*G. ruber*	Annual	3.42	[34]
MD06-3074B	17.01	124.81	-2510	North Pacific	Mg/Ca	*G. ruber*	Annual	3.17	[34]
MD07-3077	-44.15	-14.22	-3770	South Atlantic	$\delta^{18}O$	*G. bulloides*	Annual	0.77	[35]
MD07-3077	-44.15	-14.22	-3770	South Atlantic	$\delta^{18}O$	*N. pachyderma*	Annual	0.77	[35]
MD94-101	-42.50	79.42	-2920	Indian	MAT	*Na*	Seasonal	1.92	[35]
MD95-2037	37.09	-32.03	-2159	North Atlantic	$\delta^{18}O$	*G. bulloides*	Annual	2.69	[36]
MD95-2037	37.09	-32.03	-2159	North Atlantic	$U^{K'}_{37}$	*Na*	Annual	3.23	[37]
MD95-2040	40.58	-9.86	-2465	North Atlantic	$\delta^{18}O$	*G. bulloides*	Annual	0.43	[38]
MD96-2077	-33.28	31.42	-3781	Indian	$U^{K'}_{37}$	*Na*	Annual	2.88	[39]
MD96-2080	-36.27	19.48	-2488	South Atlantic	$\delta^{18}O$	*G. bulloides*	Annual	0.57	[40]
MD96-2080	-36.27	19.48	-2488	South Atlantic	Mg/Ca	*G. bulloides*	Annual	2.22	[40]
MD96-2085	-29.70	12.94	-3001	South Atlantic	$\delta^{18}O$	*Bulk*	Annual	1.42	[41]
MD96-2094	-20.00	9.27	-2280	South Atlantic	$\delta^{18}O$	*Bulk*	Annual	1.59	[42]
MD97-2120	-45.53	174.93	-1210	South Pacific	$\delta^{18}O$	*G. bulloides*	Annual	0.24	[43]
MD97-2120	-45.53	174.93	-1210	South Pacific	Mg/Ca	*G. bulloides*	Annual	0.44	[43]
MD97-2140	2.03	141.77	-2547	Equatorial Pacific	$\delta^{18}O$	*G. ruber*	Annual	3.23	[44]
MD97-2140	2.03	141.77	-2547	Equatorial Pacific	Mg/Ca	*G. ruber*	Annual	3.14	[44]
MD97-2141	8.78	121.28	-3633	Equatorial Pacific	$\delta^{18}O$	*G. ruber*	Annual	0.13	[45]
MD98-2152	-6.33	103.88	-1796	Indian	$U^{K'}_{37}$	*Na*	Annual	2.82	[46]
ML1208-16BB	0.48	-161.45	-2926	Equatorial Pacific	$\delta^{18}O$	*G. ruber*	Annual	1.58	[47]
ODP-1002	10.71	-65.17	-893	Other	$\delta^{18}O$	*G. ruber*	Annual	0.61	[48]
ODP-1012	32.28	-118.38	-1783	North Pacific	$U^{K'}_{37}$	*Na*	Annual	0.70	[18]

ODP-1020	41.00	-126.43	-3042	North Pacific	$U^{K'}_{37}$	*Na*	Annual	2.36	[18]
ODP-1059	31.68	-75.42	-2985	North Atlantic	$\delta^{18}O$	*G. ruber*	Annual	0.53	[49]
ODP-1089	-40.94	9.89	-4620.5	South Atlantic	$\delta^{18}O$	*G. bulloides*	Annual	0.61	[50]
ODP-1094	-53.18	5.13	-2807.3	South Atlantic	$\delta^{18}O$	*N. pachyderma*	Annual	0.56	[51]
ODP-1094	-53.18	5.13	-2807.3	South Atlantic	Mg/Ca	*N. pachyderma*	Annual	0.99	[51]
ODP-1123	-41.79	-171.50	-3290	South Pacific	MAT	*Na*	Annual	2.54	[52]
ODP-1125	-42.55	-178.17	-1365.1	South Pacific	$U^{K'}_{37}$	*Na*	Annual	2.96	[53]
ODP-1143	9.36	113.29	-2772.3	Equatorial Pacific	$U^{K'}_{37}$	*Na*	Annual	3.74	[54]
ODP-1144	20.05	117.42	-2037	North Pacific	$\delta^{18}O$	*G. ruber*	Annual	1.16	[55]
ODP-1144	20.05	117.42	-2037	North Pacific	Mg/Ca	*T. sacculifer*	Annual	1.16	[56]
ODP-1146	19.46	116.27	-2091.5	North Pacific	$\delta^{18}O$	*G. ruber*	Annual	0.81	[57]
ODP-1146	19.46	116.27	-2091.5	North Pacific	$U^{K'}_{37}$	*Na*	Annual	1.22	[58]
ODP-1239	-0.67	-82.08	-1414	Equatorial Pacific	$U^{K'}_{37}$	*Na*	Annual	2.37	[59]
ODP-1240	0.02	-86.45	-2920	Equatorial Pacific	$\delta^{18}O$	*G. ruber*	Annual	0.40	[60]
ODP-1240	0.02	-86.45	-2920	Equatorial Pacific	Mg/Ca	*G. ruber*	Annual	1.78	[60]
ODP-607-V30-97	41.00	-32.96	-3427	North Atlantic	MAT	*Na*	Seasonal	2.26	[61]
ODP-662	-1.39	-11.74	-3814	Equatorial Atlantic	$U^{K'}_{37}$	*Na*	Annual	1.88	[58]
ODP-677	1.20	-83.73	-3450	Equatorial Pacific	$\delta^{18}O$	*Bulk*	Annual	2.57	[62]
ODP-722	16.62	59.80	-2033.5	Indian	$U^{K'}_{37}$	*Na*	Annual	1.72	[58]
ODP-806	0.32	159.36	-2519.9	Equatorial Pacific	$\delta^{18}O$	*G. ruber*	Annual	2.30	[63]
ODP-806	0.32	159.36	-2519.9	Equatorial Pacific	Mg/Ca	*G. ruber*	Annual	3.40	[63]
ODP-846	-3.10	-90.82	-3296	Equatorial Pacific	$U^{K'}_{37}$	*Na*	Annual	2.60	[58]
ODP-871	5.55	172.35	-1255	Equatorial Pacific	Mg/Ca	*G. ruber*	Annual	2.81	[64]

ODP-980	55.48	-14.70	-2180	North Atlantic	$\delta^{18}O$	*N. pachyderma*	Annual	3.74	[65]
ODP-982	57.50	-15.87	-1135	North Atlantic	$\delta^{18}O$	*G. bulloides*	Annual	2.68	[66]
ODP-982	57.50	-15.87	-1135	North Atlantic	$U^{K'}_{37}$	*Na*	Seasonal	3.80	[66]
ODP-999	12.75	-78.73	-2827	Other	$\delta^{18}O$	*G. ruber*	Annual	1.42	[67]
ODP-999	12.75	-78.73	-2827	Other	Mg/Ca	*G. ruber*	Annual	1.43	[67]
PRGL1	42.69	3.84	-298.5	Other	$\delta^{18}O$	*G. bulloides*	Annual	0.92	[68]
PRGL1	42.69	3.84	-298.5	Other	$U^{K'}_{37}$	*Na*	Annual	0.84	[69]
PS2082	-43.22	11.74	-4610	South Atlantic	MAT	*Na*	Seasonal	3.86	[70]
PS2489-2	-42.87	8.97	-3794	South Atlantic	MAT	*Na*	Seasonal	2.59	[71]
RC11-120	-43.52	79.87	-3193	Indian	$\delta^{18}O$	*G. bulloides*	Annual	1.68	[72]
RC11-120	-43.52	79.87	-3193	Indian	MAT	*Na*	Seasonal	1.68	[72]
RC11-120	-43.52	79.87	-3193	Indian	Mg/Ca	*G. bulloides*	Annual	3.48	[33]
RC12-294	-37.27	-10.10	-3308	South Atlantic	MAT	*Na*	Seasonal	2.00	[16]
RC13-110	-0.10	-95.65	-3231	Equatorial Pacific	$\delta^{18}O$	*Bulk*	Annual	2.37	[73]
RC13-228	-22.33	11.20	-3204	South Atlantic	MAT	*Na*	Seasonal	1.78	[74]
RC27-61	16.63	59.86	-455	Indian	$\delta^{18}O$	*T. sacculifer*	Annual	3.49	[75]
SO136-111	-56.67	160.23	-3912	South Pacific	$\delta^{18}O$	*N. pachyderma*	Annual	1.56	[76]
SO136-GC3	-42.30	169.80	-1.955	South Pacific	$\delta^{18}O$	*G. bulloides*	Annual	2.08	[77]
SO136-GC3	-42.30	169.80	-1.955	South Pacific	$U^{K'}_{37}$	*Na*	Annual	1.58	[77]
SU90-39	52.57	-21.94	-3955	North Atlantic	MAT	*Na*	Seasonal	0.57	[74]
TN057-06	-42.90	8.90	-3751	South Atlantic	$\delta^{18}O$	*G. bulloides*	Annual	1.64	[78]
TR163-19	2.26	-90.95	-2348	Equatorial Pacific	$\delta^{18}O$	*G. ruber*	Annual	1.75	[79]
TR163-19	2.26	-90.95	-2348	Equatorial Pacific	Mg/Ca	*G. ruber*	Annual	1.20	[79]
U1313	41.00	-32.96	-3426	North Atlantic	$U^{K'}_{37}$	*Na*	Annual	3.09	[80]

U1385	37.57	-10.13	-2587	North Atlantic	$\delta^{18}O$	*G. bulloides*	Annual	0.18	[81]
U1385	37.57	-10.13	-2587	North Atlantic	MAT	*Na*	Annual	0.20	[82]
U1429	31.62	129.00	-732	North Pacific	$\delta^{18}O$	*G. ruber*	Annual	0.23	[83]
U1429	31.62	129.00	-732	North Pacific	Mg/Ca	*G. ruber*	Annual	0.23	[83]
U1429	31.62	129.00	-732	North Pacific	$U^{K'}_{37}$	*Na*	Annual	0.23	[83]
U1446	19.08	85.74	-1430	Indian	$\delta^{18}O$	*G. ruber*	Annual	1.20	[84]
U1446	19.08	85.74	-1430	Indian	Mg/Ca	*G. ruber*	Annual	2.84	[84]
V19-30	-3.38	-83.52	-3091	Equatorial Pacific	$\delta^{18}O$	*Bulk*	Annual	0.91	[73]

[1] Elmore et al., 2015; [2] Scussolini et al., 2013; [3] Howard et al., 1992; [4] Le et al., 1992; [5] Wefer et al., 1996; [6] Schneider et al., 1995; [7] Wefer et al., 1999; [8] Nürnberg et al., 2000; [9] Sarnthein et al., 1994; [10] Ho et al., 2012; [11] Peeters et al., 2004; [12] Candy et al., 2018; [13] Nascimento et al., 2021; [14] Rouyer-Denimal et al., 2023; [15] Imbrie et al., 1992; [16] Imbrie et al., 1989; [17] Zhang et al., 2021; [18] Herbert et al., 2001; [19] Nürnberg, 2022; [20] Holbourn et al., 2005; [21] Gebhardt et al., 2008; [22] Martrat et al., 2007; [23] Desprat et al., 2006; [24] Viveen et al., 2013; [25] Rincón-Martínez et al., 2010; [26] Nürnberg et al., 2008; [27] Romero et al., 2015; [28] Ziegler et al., 2010; [29] Li et al., 2009; [30] He et al., 2008; [31] Tachikawa et al., 2014; [32] Lo et al., 2017; [33] Mashiotta et al., 1999; [34] Jia et al., 2018; [35] This study; [36] Bahr et al., 2015; [37] Calvo et al., 2001; [38] Voelker et al., 2011; [39] Bard et al., 2009; [40] Martínez-Méndez et al., 2010; [41] Chen et al., 2002; [42] Stuut et al., 2002; [43] Pahnke et al., 2003; [44] de Garidel-Thoron et al., 2005; [45] Oppo et al., 2003; [46] Windler et al., 2019; [47] Jacobel et al., 2025; [48] Gibson et al., 2014; [49] Billups et al., 2014; [50] Hodell et al., 2003; [51] Hasenfratz et al., 2019; [52] Hayward et al., 2008; [53] Peterson et al., 2020; [54] Li et al., 2011; [55] Bühring et al., 2004; [56] Wei et al., 2007; [57] Caballero-Gill et al., 2012; [58] Herbert et al., 2010; [59] Dyez et al., 2016; [60] Pena et al., 2008; [61] Ruddiman et al., 1989; [62] Shackleton et al., 1990; [63] Medina-Elizalde et al., 2005; [64] Dyez et al., 2014; [65] McManus et al., 1999; [66] Venz et al., 1999; [67] Schmidt et al., 2006; [68] Frigola et al., 2012; [69] Cortina et al., 2015; [70] Brathauer, 1996; [71] Becquey et al., 2003; [72] Martinson et al., 1987; [73] Lyle et al., 2002; [74] Vogelsang et al., 2000; [75] Clemens et al., 1990; [76] Crosta et al., 2004; [77] Pelejero et al., 2006; [78] Hodell et al., 2000; [79] Lea, 2004; [80] Naafs et al., 2012; [81] Hodell et al., 2022; [82] Singh et al., 2024; [83] Clemens et al., 2018; [84] Clemens et al., 2021.

References

Bahr, A., Kaboth, S., Jiménez-Espejo, F. J., Sierro, F. J., Voelker, A. H., Lourens, L., ... & Friedrich, O. (2015). Persistent monsoonal forcing of Mediterranean Outflow Water dynamics during the late Pleistocene. Geology, 43(11), 951-954.

Bard, E., & Rickaby, R. E. (2009). Migration of the subtropical front as a modulator of glacial climate. Nature, 460(7253), 380-383.

Becquey, S., & Gersonde, R. (2003). A 0.55-Ma paleotemperature record from the Subantarctic zone: Implications for Antarctic Circumpolar Current development. Paleoceanography, 18(1).

Billups, K., & Scheinwald, A. (2014). Origin of millennial-scale climate signals in the subtropical North Atlantic. Paleoceanography, 29(6), 612-627.

Bouchet, M., Landais, A., Grisart, A., Parrenin, F., Prié, F., Jacob, R., Fourré, E., Capron, E., Raynaud, D., Lipenkov, V. Y., Loutre, M.-F., Extier, T., Svensson, A., Legrain, E., Martinerie, P., Leuenberger, M., Jiang, W., Ritterbusch, F., Lu, Z.-T., and Yang, G.-M.: The Antarctic Ice Core Chronology 2023 (AICC2023) chronological framework and associated timescale for the European Project for Ice Coring in Antarctica (EPICA) Dome C ice core, Clim. Past, 19, 2257–2286, https://doi.org/10.5194/cp-19-2257-2023

Brathauer, U. (1996). Rekonstruktion quartärer Klimaänderungen im atlantischen Sektor des Südpolarmeeres anhand von Radiolarien = Radiolarians as indicators for Quaternary climatic changes in the Southern Ocean (Atlantic sector) (Doctoral dissertation, Universität Bremen).

Bühring, C., Sarnthein, M., & Erlenkeuser, H. (2004, December). Toward a high-resolution stable isotope stratigraphy of the last 1.1 my: Site 1144, South China Sea. In Proc. ODP, Sci. Results (Vol. 184, pp. 1-29).

Caballero-Gill, R. P., Clemens, S. C., & Prell, W. L. (2012). Direct correlation of Chinese speleothem δ18O and South China Sea planktonic δ18O: transferring a speleothem chronology to the benthic marine chronology. Paleoceanography, 27(2).

Calvo, E., Villanueva, J., Grimalt, J. O., Boelaert, A., & Labeyrie, L. (2001). New insights into the glacial latitudinal temperature gradients in the North Atlantic. Results from UK′ 37 sea surface temperatures and terrigenous inputs. Earth and Planetary Science Letters, 188(3-4), 509-519.

Candy, I., & Alonso-Garcia, M. (2018). A 1 Ma sea surface temperature record from the North Atlantic and its implications for the early human occupation of Britain. Quaternary Research, 90(2), 406-417.

Chen, M. T., Chang, Y. P., Chang, C. C., Wang, L. W., Wang, C. H., & Yu, E. F. (2002). Late Quaternary sea-surface temperature variations in the southeast Atlantic: a planktic foraminifer faunal record of the past 600 000 yr (IMAGES II MD962085). Marine Geology, 180(1-4), 163-181.

Clemens, S. C., & Prell, W. L. (1990). Late Pleistocene variability of Arabian Sea summer monsoon winds and continental aridity: Eolian records from the lithogenic component of deep-sea sediments. Paleoceanography, 5(2), 109-145.

189 Clemens, S. C., Holbourn, A., Kubota, Y., Lee, K. E., Liu, Z., Chen, G., ... & Fox-Kemper, B. (2018). Precession-
190 band variance missing from East Asian monsoon runoff. Nature Communications, 9(1), 3364.

191 Clemens, S. C., Yamamoto, M., Thirumalai, K., Giosan, L., Richey, J. N., Nilsson-Kerr, K., ... & McGrath, S. M.
192 (2021). Remote and local drivers of Pleistocene South Asian summer monsoon precipitation: A test for future
193 predictions. Science Advances, 7(23), eabg3848.

194 Cortina, A., Sierro, F. J., Flores, J. A., Martrat, B., & Grimalt, J. O. (2015). The response of SST to insolation and
195 ice sheet variability from MIS 3 to MIS 11 in the northwestern Mediterranean Sea (Gulf of Lions). Geophysical
196 Research Letters, 42(23), 10-366.

197 Crosta, X., Sturm, A., Armand, L., & Pichon, J. J. (2004). Late Quaternary sea ice history in the Indian sector of
198 the Southern Ocean as recorded by diatom assemblages. Marine Micropaleontology, 50(3-4), 209-223.

199 de Garidel-Thoron, T., Rosenthal, Y., Bassinot, F., & Beaufort, L. (2005). Stable sea surface temperatures in the
200 western Pacific warm pool over the past 1.75 million years. Nature, 433(7023), 294-298.

201 Desprat, S., Goñi, M. F. S., Turon, J. L., Duprat, J., Malaizé, B., & Peypouquet, J. P. (2006). Climatic variability
202 of Marine Isotope Stage 7: direct land–sea–ice correlation from a multiproxy analysis of a north-western Iberian
203 margin deep-sea core. Quaternary Science Reviews, 25(9-10), 1010-1026.

204 Dyez, K. A., & Ravelo, A. C. (2014). Dynamical changes in the tropical Pacific warm pool and zonal SST gradient
205 during the Pleistocene. Geophysical Research Letters, 41(21), 7626-7633.

206 Dyez, K. A., Ravelo, A. C., & Mix, A. C. (2016). Evaluating drivers of Pleistocene eastern tropical Pacific sea
207 surface temperature. Paleoceanography, 31(8), 1054-1069.

208 Elmore, A. C., Wright, J. D., & Chalk, T. B. (2015). Precession-driven changes in Iceland–Scotland Overflow
209 Water penetration and bottom water circulation on Gardar Drift since ~200 ka. Palaeogeography,
210 Palaeoclimatology, Palaeoecology, 440, 551-563.

211 Frigola, J., Canals, M., Cacho, I., Moreno, A., Sierro, F. J., Flores, J. A., ... & Schneider, R. (2012). A 500 kyr
212 record of global sea-level oscillations in the Gulf of Lion, Mediterranean Sea: new insights into MIS 3 sea-level
213 variability. Climate of the Past, 8(3), 1067-1077.

214 Gebhardt, H., Sarnthein, M., Grootes, P. M., Kiefer, T., Kuehn, H., Schmieder, F., & Röhl, U. (2008). Paleonutrient
215 and productivity records from the subarctic North Pacific for Pleistocene glacial terminations I to V.
216 Paleoceanography, 23(4).

217 Gibson, K. A., & Peterson, L. C. (2014). A 0.6 million year record of millennial-scale climate variability in the
218 tropics. Geophysical Research Letters, 41(3), 969-975.

219 Hasenfratz, A. P., Jaccard, S. L., Martínez-García, A., Sigman, D. M., Hodell, D. A., Vance, D., ... & Haug, G. H.
220 (2019). The residence time of Southern Ocean surface waters and the 100,000-year ice age cycle. Science,
221 363(6431), 1080-1084.

Hayward, B. W., Scott, G. H., Crundwell, M. P., Kennett, J. P., Carter, L., Neil, H. L., ... & Li, Q. (2008). The effect of submerged plateaux on Pleistocene gyral circulation and sea-surface temperatures in the Southwest Pacific. Global and Planetary Change, 63(4), 309-316.

He, J., Zhao, M., Li, L., Wang, P., & Ge, H. (2008). Sea surface temperature and terrestrial biomarker records of the last 260 ka of core MD05-2904 from the northern South China Sea. Chinese Science Bulletin, 53(15), 2376-2384.

Herbert, T. D., Schuffert, J. D., Andreasen, D., Heusser, L, Lyle, M., Mix, A., ... & Herguera, J. C. (2001). Collapse of the California Current during glacial maxima linked to climate change on land. Science, 293(5527), 71-76.

Herbert, T. D., Peterson, L. C., Lawrence, K. T., & Liu, Z. (2010). Tropical ocean temperatures over the past 3.5 million years. Science, 328(5985), 1530-1534.

Hodell, D. A., Charles, C. D., & Ninnemann, U. S. (2000). Comparison of interglacial stages in the South Atlantic sector of the Southern Ocean for the past 450 kyr: implications for Marine Isotope Stage (MIS) 11. Global and Planetary Change, 24(1), 7-26.

Hodell, D. A., Charles, C. D., Curtis, J. H., Mortyn, P. G., Ninnemann, U. S., & Venz, K. A. (2003, January). Data report: Oxygen isotope stratigraphy of ODP Leg 177 Sites 1088, 1089, 1090, 1093, and 1094. In Proc. Ocean Drill. Program Sci. Results (Vol. 177, pp. 1-26).

Hodell, D., Crowhurst, S., Lourens, L., Margari, V., Nicolson, J., Rolfe, J. E., ... & Wolff, E. W. (2022). A 1.5-million-year record of orbital and millennial climate variability in the North Atlantic. Climate of the Past Discussions, 2022, 1-58.

Ho, S. L., Mollenhauer, G., Lamy, F., Martínez-Garcia, A., Mohtadi, M., Gersonde, R., ... & Tiedemann, R. (2012). Sea surface temperature variability in the Pacific sector of the Southern Ocean over the past 700 kyr. Paleoceanography, 27(4).

Holbourn, A., Kuhnt, W., Kawamura, H., Jian, Z., Grootes, P., Erlenkeuser, H., & Xu, J. (2005). Orbitally paced paleoproductivity variations in the Timor Sea and Indonesian Throughflow variability during the last 460 kyr. Paleoceanography, 20(3).

Howard, W. R., & Prell, W. L. (1992). Late Quaternary surface circulation of the southern Indian Ocean and its relationship to orbital variations. Paleoceanography, 7(1), 79-117.

Imbrie, J., Boyle, E. A., Clemens, S. C., Duffy, A., Howard, W. R., Kukla, G., ... & Toggweiler, J. R. (1992). On the structure and origin of major glaciation cycles 1. Linear responses to Milankovitch forcing. Paleoceanography, 7(6), 701-738.

Imbrie, J., McIntyre, A., & Mix, A. (1989). Oceanic response to orbital forcing in the late Quaternary: Observational and experimental strategies. In Climate and Geo-sciences: a Challenge for Science and Society in the 21st Century (pp. 121-164). Dordrecht: Springer Netherlands.

Jacobel, A. W., Costa, K. M., Applebaum, L. M., & Conde, S. (2025). New controls on sedimentation and climate in the central equatorial Pacific Ocean. Geochronology, 7(1), 123-138.

Jia, Q., Li, T., Xiong, Z., Steinke, S., Jiang, F., Chang, F., & Qin, B. (2018). Hydrological variability in the western tropical Pacific over the past 700 kyr and its linkage to Northern Hemisphere climatic change. Palaeogeography, Palaeoclimatology, Palaeoecology, 493, 44-54.

Jouzel, J., Masson-Delmotte, V., Cattani, O., Dreyfus, G., Falourd, S., Hoffmann, G., Minster, B., Nouet, J., Barnola, J. M., Chappellaz, J., Fischer, H., Gallet, J. C., Johnsen, S., Leuenberger, M., Loulergue, L., Luethi, D., Oerter, H., Parrenin, F., Raisbeck, G., Raynaud, D., Schilt, A., Schwander, J., Selmo, E., Souchez, R., Spahni, R., Stauffer, B., Steffensen, J. P., Stenni, B., Stocker, T. F., Tison, J. L., Werner, M., and Wolff, E. W. (2007): Orbital and Millennial Antarctic Climate Variability over the Past 800,000 Years, Science, 317, 793–796, https://doi.org/10.1126/science.1141038

Le, J., & Shackleton, N. J. (1992). Carbonate dissolution fluctuations in the western equatorial Pacific during the late Quaternary. Paleoceanography, 7(1), 21-42.

Lea, D. W. (2004). The 100 000-yr cycle in tropical SST, greenhouse forcing, and climate sensitivity. Journal of Climate, 17(11), 2170-2179.

Li, L., Wang, H, Li, J., Zhao, M., & Wang, P. (2009). Changes in sea surface temperature in western South China Sea over the past 450 ka. Chinese Science Bulletin, 54(18), 3335-3343.

Li, L., Li, Q., Tian, J., Wang, P., Wang, H., & Liu, Z. (2011). A 4-Ma record of thermal evolution in the tropical western Pacific and its implications on climate change. Earth and Planetary Science Letters, 309(1-2), 10-20.

Lo, L., Chang, S. P., Wei, K. Y., Lee, S. Y., Ou, T. H., Chen, Y. C., ... & Shen, C. C. (2017). Nonlinear climatic sensitivity to greenhouse gases over past 4 glacial/interglacial cycles. Scientific Reports, 7(1), 4626.

Lyle, M., Mix, A., & Pisias, N. (2002). Patterns of CaCO3 deposition in the eastern tropical Pacific Ocean for the last 150 kyr: Evidence for a southeast Pacific depositional spike during marine isotope stage (MIS) 2. Paleoceanography, 17(2), 3-1.

Martrat, B., Grimalt, J. O., Shackleton, N. J., de Abreu, L., Hutterli, M. A., & Stocker, T. F. (2007). Four climate cycles of recurring deep and surface water destabilizations on the Iberian margin. Science, 317(5837), 502-507.

Martinson, D. G., Pisias, N. G., Hays, J. D., Imbrie, J., Moore Jr, T. C., & Shackleton, N. J. (1987). Age dating and the orbital theory of the ice ages: development of a high-resolution 0 to 300,000-year chronostratigraphy. Quaternary Research, 27(1), 1-29.

Martínez-Méndez, G., Zahn, R., Hall, I. R., Peeters, F. J., Pena, L. D., Cacho, I., & Negre, C. (2010). Contrasting multiproxy reconstructions of surface ocean hydrography in the Agulhas Corridor and implications for the Agulhas Leakage during the last 345,000 years. Paleoceanography, 25(4).

Mashiotta, T. A., Lea, D. W., & Spero, H. J. (1999). Glacial–interglacial changes in Subantarctic sea surface temperature and δ18O-water using foraminiferal Mg. Earth and Planetary Science Letters, 170(4), 417-432.

McManus, J. F., Oppo, D. W., & Cullen, J. L. (1999). A 0.5-million-year record of millennial-scale climate variability in the North Atlantic. Science, 283(5404), 971-975.

Medina-Elizalde, M., & Lea, D. W. (2005). The mid-Pleistocene transition in the tropical Pacific. Science, 310(5750), 1009-1012.

Naafs, B. D. A., Hefter, J., Acton, G., Haug, G. H., Martínez-Garcia, A., Pancost, R., & Stein, R. (2012). Strengthening of North American dust sources during the late Pliocene (2.7 Ma). Earth and Planetary Science Letters, 317, 8-19.

Nascimento, R. A., Venancio, I. M., Chiessi, C. M., Ballalai, J. M., Kuhnert, H., Johnstone, H., ... & Albuquerque, A. L. S. (2021). Tropical Atlantic stratification response to late Quaternary precessional forcing. Earth and Planetary Science Letters, 568, 117030.

Nürnberg, D., Müller, A., & Schneider, R. R. (2000). Paleo-sea surface temperature calculations in the equatorial east Atlantic from Mg/Ca ratios in planktic foraminifera: A comparison to sea surface temperature estimates from U37K′, oxygen isotopes, and foraminiferal transfer function. Paleoceanography, 15(1), 124-134.

Nürnberg, D., Ziegler, M., Karas, C., Tiedemann, R., & Schmidt, M. W. (2008). Interacting Loop Current variability and Mississippi River discharge over the past 400 kyr. Earth and Planetary Science Letters, 272(1-2), 278-289.

Nürnberg, Dirk (2022): Benthic and planktonic stable isotopes and coarse fraction of sediment core M94-480 PC [dataset]. PANGAEA, https://doi.org/10.1594/PANGAEA.947790

Oppo, D. W., Linsley, B. K., Rosenthal, Y., Dannenmann, S., & Beaufort, L. (2003). Orbital and suborbital climate variability in the Sulu Sea, western tropical Pacific. Geochemistry, Geophysics, Geosystems, 4(1), 1-20.

Paillard, D., Labeyrie, L., and Yiou, P. (1996): Macintosh program performs time-series analysis, Eos Transactions, 77, 379–379, https://doi.org/10.1029/96EO00259

Pahnke, K., Zahn, R., Elderfield, H., & Schulz, M. (2003). 340,000-year centennial-scale marine record of Southern Hemisphere climatic oscillation. Science, 301(5635), 948-952.

Peeters, F. J., Acheson, R., Brummer, G. J. A., De Ruijter, W. P., Schneider, R. R., Ganssen, G. M., ... & Kroon, D. (2004). Vigorous exchange between the Indian and Atlantic oceans at the end of the past five glacial periods. Nature, 430(7000), 661-665.

Pelejero, C., Calvo, E., Barrows, T. T., Logan, G. A., & De Deckker, P. (2006). South Tasman Sea alkenone palaeothermometry over the last four glacial/interglacial cycles. Marine Geology, 230(1-2), 73-86.

Pena, L. D., Cacho, I., Ferretti, P., & Hall, M. A. (2008). El Niño–Southern Oscillation–like variability during glacial terminations and interlatitudinal teleconnections. Paleoceanography, 23(3).

Peterson, L. C., Lawrence, K. T., Herbert, T. D., Caballero-Gill, R., Wilson, J., Huska, K., ... & Holte, L. (2020). Plio-Pleistocene hemispheric (a)symmetries in the Northern and Southern Hemisphere midlatitudes. Paleoceanography and Paleoclimatology, 35(3), e2019PA003720.

Rincón-Martínez, D., Lamy, F., Contreras, S., Leduc, G., Bard, E., Saukel, C., ... & Tiedemann, R. (2010). More humid interglacials in Ecuador during the past 500 kyr linked to latitudinal shifts of the equatorial front and the Intertropical Convergence Zone in the eastern tropical Pacific. Paleoceanography, 25(2).

Romero, O. E., Kim, J. H., Bárcena, M. A., Hall, I. R., Zahn, R., & Schneider, R. (2015). High-latitude forcing of diatom productivity in the southern Agulhas Plateau during the past 350 kyr. Paleoceanography, 30(2), 118-132.

Rouyer-Denimal, L., Govin, A., Bouloubassi, I., Tu, T. T. N., Albuquerque, A. L. S., Anquetil, C., & Huguet, A. (2023). Subsurface warming in the tropical Atlantic for the last 3 deglaciations: Insights from organic molecular proxies. Quaternary Science Reviews, 321, 108370.

Ruddiman, W. F., Raymo, M., Martinson, D. G., Clement, B. M., & Backman, J. (1989). Pleistocene evolution: Northern Hemisphere ice sheets and North Atlantic Ocean. Paleoceanography, 4(4), 353-412.

Sarnthein, M., Winn, K., Jung, S. J., Duplessy, J. C., Labeyrie, L., Erlenkeuser, H., & Ganssen, G. (1994). Changes in east Atlantic deepwater circulation over the last 30,000 years: Eight time slice reconstructions. Paleoceanography, 9(2), 209-267.

Schmidt, M. W., Vautravers, M. J., & Spero, H. J. (2006). Western Caribbean sea surface temperatures during the late Quaternary. Geochemistry, Geophysics, Geosystems, 7(2).

Schneider, R. R., Müller, P. J., & Ruhland, G. (1995). Late Quaternary surface circulation in the east equatorial South Atlantic: Evidence from alkenone sea surface temperatures. Paleoceanography, 10(2), 197-219.

Scussolini, P., & Peeters, F. J. (2013). A record of the last 460 thousand years of upper ocean stratification from the central Walvis Ridge, South Atlantic. Paleoceanography, 28(3), 426-439.

Shackleton, N. J., Berger, A., & Peltier, W. R. (1990). An alternative astronomical calibration of the lower Pleistocene timescale based on ODP Site 677. Earth and Environmental Science Transactions of the Royal Society of Edinburgh, 81(4), 251-261.

Singh, H., & Singh, A. D. (2024). New insights into the surface-ocean dynamics of the Northeastern Atlantic Ocean across the Marine Isotope Stage 7. Paleoceanography and Paleoclimatology, 39(5), e2023PA004722.

Stuut, J. B. W., Prins, M. A., Schneider, R. R., Weltje, G. J., Jansen, J. F., & Postma, G. (2002). A 300-kyr record of aridity and wind strength in southwestern Africa: inferences from grain-size distributions of sediments on Walvis Ridge, SE Atlantic. Marine Geology, 180(1-4), 221-233.

Tachikawa, K., Timmermann, A., Vidal, L., Sonzogni, C., & Timm, O. E. (2014). CO2 radiative forcing and Intertropical Convergence Zone influences on western Pacific warm pool climate over the past 400 ka. Quaternary Science Reviews, 86, 24-34.

Venz, K. A., Hodell, D. A., Stanton, C., & Warnke, D. A. (1999). A 1.0 Myr record of Glacial North Atlantic Intermediate Water variability from ODP site 982 in the northeast Atlantic. Paleoceanography, 14(1), 42-52.

Viveen, W., Schoorl, J. M., Veldkamp, A., Van Balen, R. T., Desprat, S., & Vidal-Romani, J. R. (2013). Reconstructing the interacting effects of base level, climate, and tectonic uplift in the lower Miño River terrace record: a gradient modelling evaluation. Geomorphology, 186, 96-118.

Voelker, A. H., & de Abreu, L. (2011). A review of abrupt climate change events in the Northeastern Atlantic Ocean (Iberian Margin): Latitudinal, longitudinal, and vertical gradients. Abrupt Climate Change: Mechanisms, Patterns, and Impacts, 193, 15-37.

Vogelsang, E., Sarnthein, M., & Pflaumann, U. (2000). d18O-Stratigraphy, Chronology and Sea Surface Temperatures of Atlantic Sediment Records. Berichte: Reports.

Wei, G., Deng, W., Liu, Y., & Li, X. (2007). High-resolution sea surface temperature records derived from foraminiferal Mg/Ca ratios during the last 260 ka in the northern South China Sea. Palaeogeography, Palaeoclimatology, Palaeoecology, 250(1-4), 126-138.

Wefer, G. A., Berger, W. H., Bickert, T., Donner, B., Fischer, G., von Mücke, S. K., ... & Segl, M. (1996). Late Quaternary surface circulation of the South Atlantic: The stable isotope record and implications for heat transport and productivity. In The South Atlantic: Present and Past Circulation (pp. 461-502). Berlin, Heidelberg: Springer Berlin Heidelberg.

Wefer, G., Berger, W. H., Bijma, J., & Fischer, G. (1999). Clues to ocean history: a brief overview of proxies. Use of Proxies in Paleoceanography: Examples from the South Atlantic, 1-68.

Windler, G., Tierney, J. E., DiNezio, P. N., Gibson, K., & Thunell, R. (2019). Shelf exposure influence on Indo-Pacific Warm Pool climate for the last 450,000 years. Earth and Planetary Science Letters, 516, 66-76.

Zhang, S., Yu, Z., Gong, X., Wang, Y., Chang, F., Lohmman, G., ... & Li, T. (2021). Precession cycles of the El Niño/Southern oscillation-like system controlled by Pacific upper-ocean stratification. Communications Earth & Environment, 2(1), 239.

Ziegler, M., Lourens, L. J., Tuenter, E., & Reichart, G. J. (2010). High Arabian Sea productivity conditions during MIS 13–odd monsoon event or intensified overturning circulation at the end of the Mid-Pleistocene transition?. Climate of the Past, 6(1), 63-76.